Treatment of LBCs in 2D Simulation of Convection over Hills

Wenshou TIAN*[1], GUO Zhenhai[2] (郭振海), and YU Rucong[2] (宇如聪)

[1] *The School of Environment, University of Leeds, UK*

[2] *State Key Laboratory of Numerical Modeling for Atmospheric Sciences and Geophysical Fluid Dynamics, Institute of Atmospheric Physics, Chinese Academy of Sciences, Beijing*, 100029

(Received 3 September 2003; revised 31 December 2003)

ABSTRACT

A series of idealized model simulations are analyzed to determine the sensitivity of model results to different configurations of the lateral boundary conditions (LBCs) in simulating mesoscale shallow convection over hilly terrain. In the simulations with steady thermal forcing at the model surface, a radiation condition at both boundaries is the best choice under high wind conditions, and the best results are produced when both the normal velocities and the temperature are treated with the radiation scheme in which the phase speed is the same for different variables. When the background wind speed is reasonably small, the LBC configuration with either the radiation or the zero gradient condition at both boundaries tends to make the numerical solution unstable. The choice of a constant condition at the inflow boundary and a radiation outflow boundary condition is appropriate in most cases. In the simulations with diurnal thermal forcing at the model surface, different LBC schemes are combined together to reduce spurious signals induced by the outflow boundary. A specification inflow boundary condition, in which the velocity fields at the inflow boundary are provided using the time-dependent results of a simulation with periodic LBCs over a flat domain, is tested and the results indicate that the specification condition at the inflow boundary makes it possible to use a smaller model domain to obtain reasonable results. The model horizontal domain length should be greater than a critical length, which depends on the domain depth H and the angle between gravity wave phase lines and the vertical. An estimate of minimum domain length is given by $[(H - z_i)/\pi U]\sqrt{N^2 L_x^2 - 4\pi^2 U^2}$, where N and U are the background stability and wind speed, respectively, L_x is the typical gravity wavelength scale, and z_i is the convective boundary layer (CBL) depth.

Key words: lateral boundary condition, numerical simulation, convection, orography

1. Introduction

It has long been recognized that the treatment of lateral boundary conditions (LBCs) in convective and mesoscale modelling is extremely complicated but vifally important. Basically, there are two types of LBCs: periodic and open boundary conditions. An absorbing boundary condition, which is a crude open condition, is often used to damp unwanted reflections of waves by boundaries. However, such an absorbing layer is not an actual boundary condition. The use of a damping layer is to ensure, hopefully, that the wave reflections are eliminated if the actual boundary condition has failed to do so.

Periodic boundary conditions are computationally less problematic, but are not suitable in some problems where advection or trapped wave motions dominate. In particular, when the flow is directed over a single obstacle, where the flow properties downstream and upstream of the obstacle are different, a periodic boundary condition is not physically justified. What is needed in many problems is an open boundary condition which allows disturbances travelling outward from the interior of the model domain to propagate out of the boundary without generating spurious reflections. The commonly used open boundary condition is the Sommerfeld radiation condition (Sommerfeld, 1949, p.189), which assumes

$$\frac{\partial \phi}{\partial t} + C\frac{\partial \phi}{\partial x_n} = 0\,, \tag{1}$$

*E-mail: wenshou@env.leeds.ac.uk

where t is the time and x_n is the coordinate perpendicular to the boundary in question, ϕ is an arbitrary variable and C is the phase velocity, determination of which is still a subject of much debate.

Pearson (1974) proposed estimating from a linearized dispersion relation while Orlanski (1976) suggested calculating C locally at a point just inside the boundary from the relation

$$C = -\frac{\partial \phi}{\partial t} \Big/ \frac{\partial \phi}{\partial x_n} \,. \tag{2}$$

Clark (1979) compared the results using the Orlanski (1976) formulation and the Klemp and the Wilhelmson (1978) treatment, which uses a fixed phase speed in convective simulations, and showed that it is better to calculate C than to use a fixed value, while Durran et al. (1993) pointed out that better results were achieved by using a fixed C in the one-dimensional shallow-water problem. Some previous researchers (e.g., Miller and Thorpe, 1981; Raymond and Kuo, 1984; Miranda and James, 1992; Durran et al., 1993), however, have proposed other variants of the radiation condition based on (1) in attempts to improve the representation of the Sommerfeld radiation condition.

Apart from the radiative boundary condition, the other two commonly used boundary conditions are as follows. The zero gradient condition assumes that any variable ϕ at a lateral boundary is given by

$$\frac{\partial \phi}{\partial x_n} = 0 \,. \tag{3}$$

The other simple LBC is the constant boundary value condition, i.e.,

$$\frac{\partial \phi}{\partial t} = 0 \,. \tag{4}$$

Despite some uncertainties in the phase velocity specification, the radiative boundary condition is thought to be better than other open boundary conditions (e.g., Miller and Thorpe, 1981). However, as pointed out by Durran et al. (1993), even the perfect radiative boundary condition may be incapable of correctly mimicking the presence of the surrounding fluid at the boundary and hence introduce errors or excite local unstable modes. Clark (1979) has shown that a computational mode is strongly excited when a fixed phase speed is used in the radiation condition scheme, while an example of the inadequacy of the radiative boundary condition has been provided by Durran and Klemp (1983) in their nonlinear mountain-wave simulations. On the other hand, although the radiation condition can be applied, from a theoretical point of view, on all boundaries of the model domain for all the model variables, it has been used in combination with the zero gradient and the constant boundary value conditions in most studies. The LBCs may be different at different boundaries. Even at the same boundary, the boundary conditions need not be the same for different model variables. Clark (1979) showed that the zero gradient condition at the lateral boundaries for the treatment of non-normal velocity components may accentuate the undesirable effects of the Orlanski scheme while the arguments of Sundstrom and Elvius (1979) suggested that the constant boundary value condition for inflow was necessary for well-posed conditions. Finally, a good boundary condition configuration should be not only accurate but also stable.

No attempts will be made to improve the general merits of various radiation condition schemes. Our interests are whether there is an optimal combination of those commonly used boundary conditions for a given physical problem and how to use the radiation condition in a more appropriate way.

Two kinds of errors are generated by the boundaries in the simulation of time-dependent convection systems. One kind is related to a failure to incorporate inward proppagating signals generated by real physical processes outside of the boundaries of the model domain, and in some cases, errors at the outflow boundary are even "necessary" to mimic inward disturbances to produce desired results; the other kind of error is associated with the failure of imposed boundary conditions to properly direct all propagating signals outward through the boundaries. Errors of the first kind can be reduced through nested grids or enlarging the domain at the expense of computer resources, while the errors of the second kind can be diminished by improving the permeability of the lateral boundaries to outgoing waves. In section 3.3, we have attempted to diminish errors of second kind by using mixed boundary conditions. The effects of the model domain length on model results and the choice of domain length are also discussed.

2. Numerical experiments

The physical problem we considered is mesoscale boundary layer dry convection over a single obstacle. For simplicity, the issue will be addressed in a two dimensional configuration. The model used is the Met Office boundary layer model named BLASIUS (e.g., Mason, 1987; Wood and Mason, 1991). The numerical schemes used in the model are similar to those described by Clark (1977). The turbulence closure scheme is first-order and similar to that employed in large eddy simulations (e.g., Deardorff, 1974) except that the mixing length scale is arbitrarily chosen.

The discrete forms of the boundary conditions (1), (3), and (4) may vary depending on the finite difference scheme used. In an x-z system, their basic forms used in the model are described in the following. Note that unless otherwise stated, the term "inflow boundary" is a boundary on which the advective velocity is pointing into the domain, while "outflow boundary" is given to a boundary on which the advective velocity is pointing out of the domain. We have also assumed that the basic flow has no vertical directional shear.

(a) The radiation condition scheme is the same as that proposed by Orlanski (1976). At the right boundary, with index b, first assuming $\partial\phi/\partial t$ centered at $(b-1, n-1)$, i.e.,

$$\frac{\partial \phi}{\partial t} = \frac{\phi_{b-1,n} - \phi_{b-1,n-2}}{2\Delta t} \tag{5}$$

and $\partial\phi/\partial x$ discreted as

$$\frac{\partial \phi}{\partial x} = \frac{\phi_{b-1,n} + \phi_{b-1,n-2} - 2\phi_{b-2,n-1}}{2\Delta x} , \tag{6}$$

then (2) can be approximated by

$$C = \frac{\Delta x}{\Delta t} \frac{\phi_{b-1,n-2} - \phi_{b-1,n}}{\phi_{b-1,n} + \phi_{b-1,n-2} - 2\phi_{b-2,n-1}} , \tag{7}$$

where $\phi_{b,n}$ is at the boundary point b, at time n. Appropriate limits for C are employed, as used by Miranda and James (1992), for extremities. The finite difference replacement of (1) with $\partial\phi/\partial t$ centered at (b, n) is given by

$$\phi_{b,n+1} = \phi_{b,n-1} - C\frac{\Delta t}{\Delta x}(\phi_{b,n+1} + \phi_{b,n-1} - 2\phi_{b-1,n}) . \tag{8}$$

Rewriting (7) and (8), we get the governing equation for variable ϕ at the right boundary

$$\phi_{b,n+1} = \frac{\phi_{b,n-1}(1 - r_\phi) + 2r_\phi\phi_{b-1,n}}{1 + r_\phi} \tag{9}$$

where r_ϕ is given by

$$r_\phi = \frac{\phi_{b-1,n-2} - \phi_{b-1,n}}{\phi_{b-1,n} + \phi_{b-1,n-2} - 2\phi_{b-2,n-1}} . \tag{10}$$

For the left boundary, with index $b = 0$, the above two equations become:

$$\phi_{b,n+1} = \frac{\phi_{b,n-1}(1 + r_\phi) - 2r_\phi\phi_{b+1,n}}{1 - r_\phi} , \tag{11}$$

$$r_\phi = \frac{\phi_{b+1,n-2} - \phi_{b+1,n}}{-\phi_{b+1,n} - \phi_{b+1,n-2} + 2\phi_{b+2,n-1}} . \tag{12}$$

In our model, the radiative boundary condition is only applied on the velocity components in the two dimensional x-z plane and on the temperature, and the phase speed C is calculated from the horizontal velocity field u. For all the other variables, the zero gradient condition is imposed unless otherwise stated.

(b) The zero gradient condition is discretized as follows:

$$\phi_{b,n+1} = \phi_{b+1,n+1} \quad \text{for} \quad b = 0 , \tag{13}$$

$$\phi_{b,n+1} = \phi_{b-1,n+1} \quad \text{for} \quad b = N_x , \tag{14}$$

where N_x is the number of grid points.

(c) For the constant boundary value condition, the boundary value of a variable is set to its initial value. In our model, the constant boundary value condition is only applied on horizontal velocities, while conservation of the mass is applied at the outflow if the opposite boundary adopts a constant boundary value condition, to ensure that the mass flux is the same at both inflow and outflow boundaries. In the x-z plane, the mass flux is defined by

$$\int_0^H \int_0^L u dz dy , \tag{15}$$

the velocity is then corrected by a factor:

$$\frac{1}{HL}\int_0^H \int_0^L (u_{b,n+1} - u_{\rm i}) dz dy , \tag{16}$$

where $u_{\rm i}$ is the initial value. H and L are the domain length and depth, respectively.

(d) A "specification" boundary condition has been constructed in which the boundary values of velocity at the inflow are specified using the results of a simulation in a flat domain with periodic boundary conditions. More specifically, we take a vertical section at the mid point of the domain every minute from the periodic run, and use that as the inflow for the corresponding time in the hilly run. In this case, the mass conservation constraint is also imposed.

In each of these open boundary conditions, the discretization scheme yields small errors at the boundaries in a time-dependent solution, even in the case of an initially uniform flow over flat terrain. The result of this is to generate convective instabilities originating from the boundaries, where there would be no such motion in a periodic solution.

For simplicity, the upper boundary condition is fixed for all experiments. Five types of the LBC configuration, listed in Table 1, are checked in this study. The periodic boundary condition is included for comparison. Two background wind speeds were used, i.e.,

Table 1. The LBC configurations for the numerical experiments.

Configurations	Inflow	Outflow
RR	Radiation	Radiation
ZZ	Zero gradient	Zero gradient
CR	Constant value	Radiation
ZR	Zero gradient	Radiation
CZ	Constant value	Zero gradient
PP	Periodic	Periodic

$2\,\mathrm{m\,s^{-1}}$ and $10\,\mathrm{m\,s^{-1}}$, which represent light wind conditions and higher wind conditions respectively. The domain depth is 10 km for all runs. A domain of 40-km length is used in most of the runs, and domains of length 60 km and 80 km will be used in some reference runs.

3. Results and discussion

3.1 *Case 1: flat terrain with constant surface thermal forcing*

Before discussing the simulations performed over a single hill, it is instructive to check the results over flat terrain. Figure 1 shows the time evolution of the spatially averaged vertical velocity variance $\overline{w}^2_{x,z}$ obtained from the simulations with different LBC configurations. It can be noted from the figure that even without any perturbations added to the initial temperature field, the simulations with open boundary conditions can generate vertical motions which are excited by the errors introduced at the boundaries. The time at which resolved vertical motions are triggered is different between simulations with different LBC configurations and different large scale geostrophic winds. When the inflow boundary condition is zero gradient, the vertical motions begin to set in at the simulation time 160 minutes under high wind conditions (Fig. 1a) and 100 minutes under light wind conditions (Fig. 1b). For other LBC configurations, vertical motions appear much earlier, approximately after 80–90 minutes of simulation for both high and light background winds.

The magnitudes of these computationally triggered vertical motions have large variations with simulation time when background winds are high while vertical motions are rather persistent and self-sustaining under light background winds. Figure 1a indicates that the model solution is more stable when the inflow and outflow boundary conditions are both radiation or the zero gradient condition than when the inflow and outflow boundary conditions are not the same. Figure 1b, however suggests no pronounced superiority of configurations RR or ZZ over the others. Also noticeable is that although the zero gradient condition at inflow introduces smaller errors than the other LBCs do, the corresponding error induced mode has the largest growth rate.

It should be stressed again that vertical motions in Fig. 1 are computationally induced modes since there are no perturbations added to the initial model fields in those simulations. To further clarify the model behavior with different LBC configurations, the simulations in Fig. 1 were rerun with a randomly perturbated initial temperature field identical to that in corresponding simulations over flat periodic domain. Under such circumstances, the periodic solution can be regarded

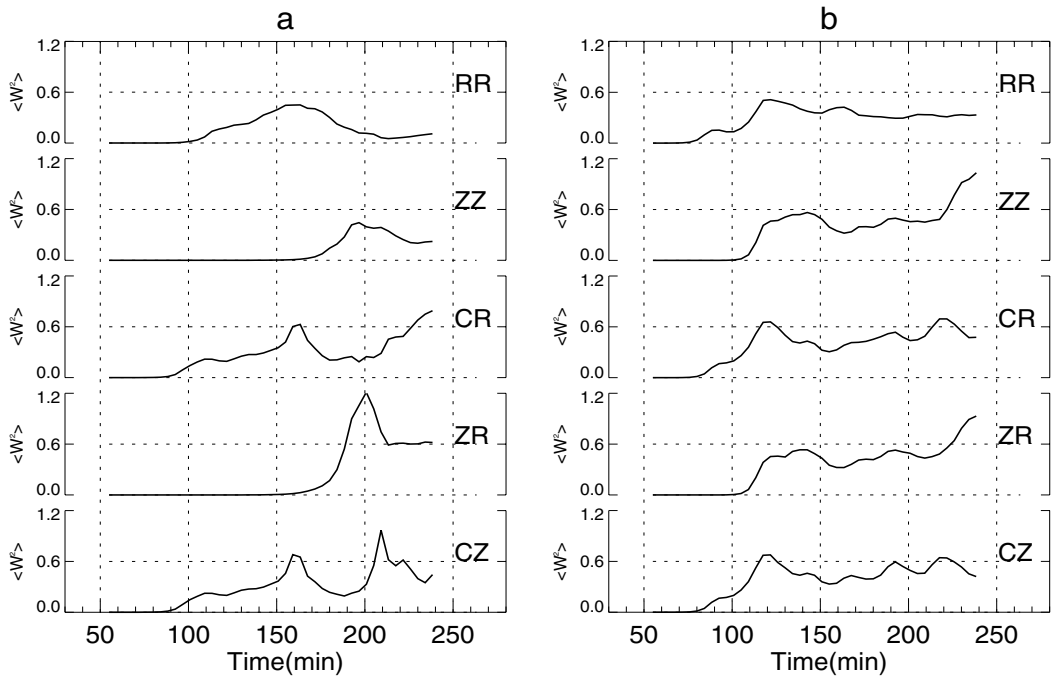

Fig. 1. The time evolution of the spatially averaged vertical velocity variance obtained from the flat-terrain simulations with the LBC configurations RR–CZ. The large scale geostrophic winds are (a) $10\,\mathrm{m\,s^{-1}}$ and (b) $2\,\mathrm{m\,s^{-1}}$.

as the reference to the solutions with open LBCs. Figure 2 shows the time evolution of the spatially averaged vertical velocity variance, $\overline{w}^2_{x,z}$ obtained from those simulations which all have the same model configuration except LBCs. The figure indicates that the ZZ configuration gives a relatively poor solution while the RR configuration does the best job throughout the simulation compared with the periodic solution. The configuration CR also gives reasonable results within 200 minutes of simulation regardless of the background wind conditions.

Figure 3 shows the domain-averaged horizontal velocity u from the corresponding simulations in Fig. 2. One can note that under both light and high wind conditions, the CR configuration works well while the ZZ configuration gives unstable solutions. The RR configuration does a good job under high wind conditions but performs poorly under light wind conditions. Recall that the RR configuration also appears to be a good one under light wind conditions with regard to the vertical velocity field (Fig. 2b).

From the above analysis we can note that the RR configuration is the best configuration only under high wind conditions in terms of the numerical stability for the velocity fields (Fig. 2a, and Fig. 3a). Under both high and light wind conditions, the CR configuration is stable for a relatively long simulation time. Caution must be taken when we attempt to seek the quasi-steady state model solution with open LBCs because there will be an interaction between convection and boundary-induced perturbations: the unstable CBL provides a source of energy on which boundary errors will grow, and conversely, convective eddies will lead to errors when they meet a boundary. One can expect a reasonably accurate physical solution only when the simulation time t is less than some critical value t_c. A t_c of about 150 minutes is noticeable in the above simulations and it is not significantly sensitive to the background winds or the LBCs.

3.2 *Case 2: hilly terrain, constant surface thermal forcing*

The numerical experiments performed over a hilly terrain are the same as those over a flat terrain except that there are no random perturbations added to the initial potential temperature field. Strictly speaking, simulations with a hill in the model domain but with periodic LBCs at horizontal boundaries actually means that the simulation is performed over an infinite domain with a range of hills in it, but simulations with open boundary conditions can be associated with the problem of flow over a single hill. However, the periodic solution over a relatively large domain with a small hill centred in it can still be regarded as a reference to solutions with open boundary conditions. In

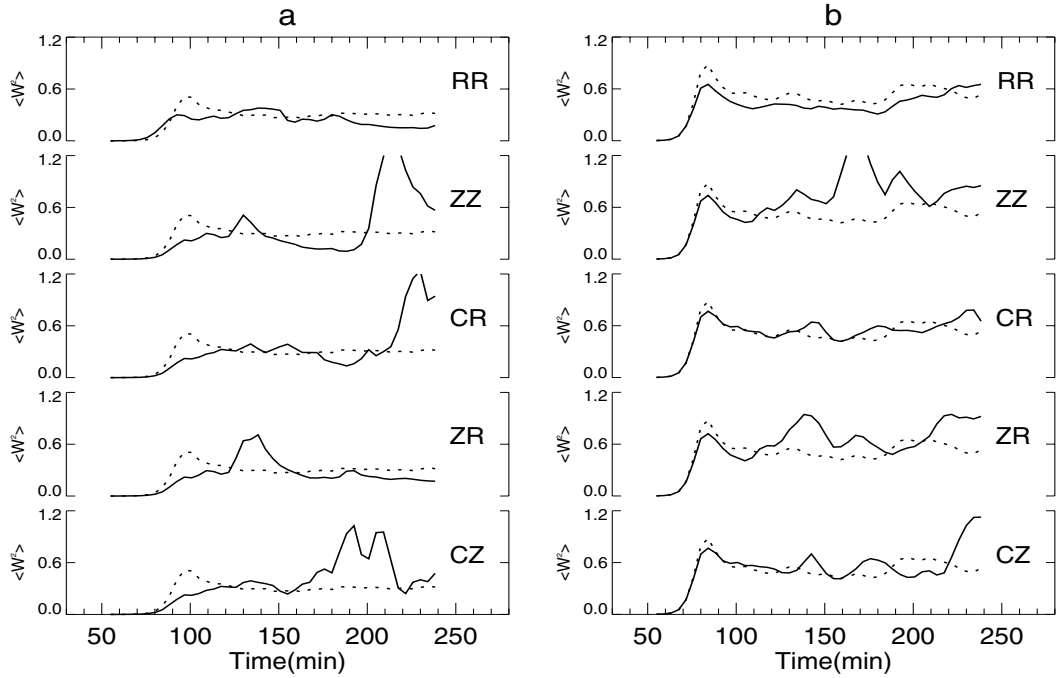

Fig. 2. As in Fig. 1, but for the simulations which are started with the initial potential temperature randomly perturbated. The periodic solution is superposed as a dotted line. The large scale geostrophic winds are (a) 10 m s^{-1} and (b) 2 m s^{-1}.

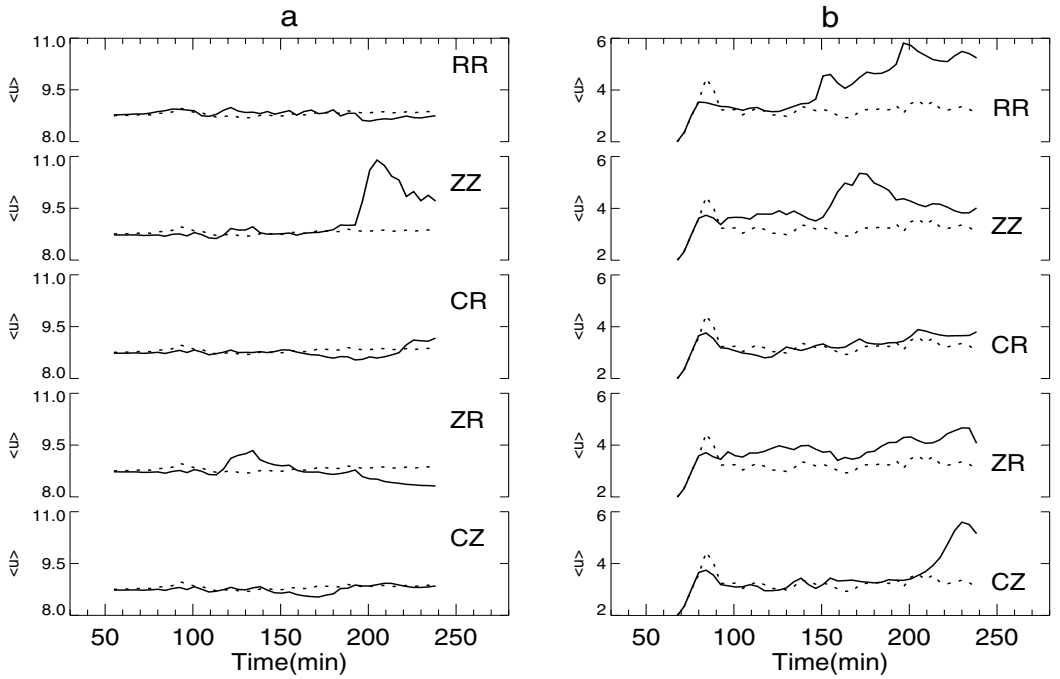

Fig. 3. The domain-averaged horizontal velocity u from corresponding simulations in Fig. 2. The large scale geostrophic winds are (a) 10 m s^{-1} and (b) 2 m s^{-1}.

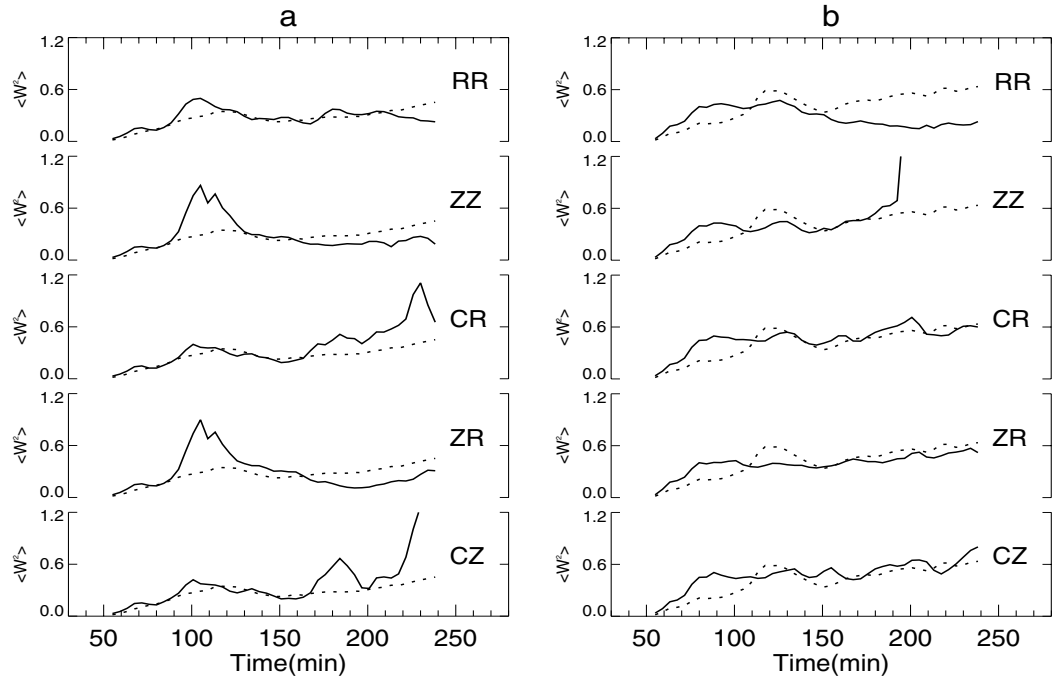

Fig. 4. As in Fig. 1, but for simulations over hilly terrain.

this section, the domain length of periodic simulations is enlarged to 80 km, and a 200-m high and 10-km wide hill is centered in the model domain in all simulations.

Analogous to Fig. 1, Fig. 4 shows the time evolution of spatially averaged vertical velocity variance $\overline{w}^2_{x,z}$ obtained from hilly terrain simulations. Under high wind conditions (Fig. 4a), the RR configuration gives the best prediction of $\overline{w}^2_{x,z}$ throughout the simulation and

the CR and CZ configurations also work well for the first 150 minutes of the simulation. A rapid increase in $\overline{w}^2_{x,z}$ at the initial stage of the simulation can be noted when the zero gradient condition is imposed at the inflow boundary (ZZ, ZR) and an increase of $\overline{w}^2_{x,z}$ at the final stage of the simulation is evident when the constant value condition is used at the inflow boundary (CR, CZ). These features are consistent with the results from the flat terrain simulations although the time of the occurrence of those peaks and troughs in $\overline{w}^2_{x,z}$ is different because the characteristics of the perturbations imposed on the model fields are different in the flat and hill terrain runs.

When the background wind speeds are small, Fig. 4b suggests that the results are not acceptable for the RR and ZZ configurations, while the results corresponding to the CR, ZR, and CZ configurations are more consistent with the periodic solution over a large domain.

The horizontal velocity fields from corresponding simulations in Fig. 4 also indicate that the RR and ZZ configurations give unstable solutions when the background winds are small (Fig. 5b). It is apparent that use of the radiation boundary condition at both boundaries is not always justified. One can note from Fig. 5a that the horizontal velocity field associated with the RR configuration is even less accurate than that with the CR configuration although the vertical velocity field associated with the RR configuration is the best in Fig. 4a. An interesting point here is that an LBC configuration may be good with respect to one model variable, but is unstable for another model variable.

It is apparent that the CR configuration is the best choice under both high and light background wind conditions. Although the ZR configuration also seems to be acceptable, it gives rise to a large jump in vertical velocity variance at the beginning of convection development under high background winds (Fig. 4a). In a simulation of developing convective systems, such an artificial jump will possibly trigger spurious moist convective modes.

One problem arising from the CR configuration is that the flow tends to reverse in simulations under light background winds. Figure 6 shows the Hovmöller diagrams of the column averaged horizontal velocities, $\overline{u}_z$, from two simulations under light wind conditions: one is performed over a large domain (80 km) with periodic LBCs, and the other is performed over the standard domain (40 km) with the LBC configuration CR. Compared with the large periodic domain solution (Fig. 6a), the solution with the CR configuration loses reliability gradually near the inflow boundary when convection begins to set in. According to our definition of inflow and outflow boundaries, this flow reversal will change the character of the physical problem by turning the inflow boundary into an outflow boundary.

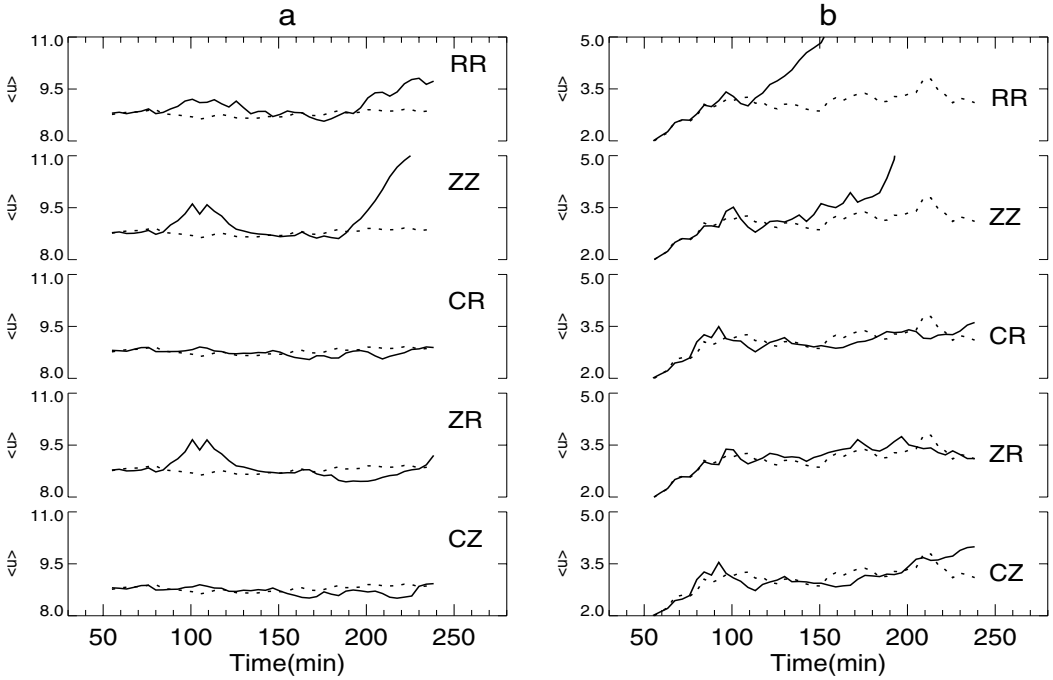

Fig. 5. As in Fig. 3, but for experiments over hilly terrain.

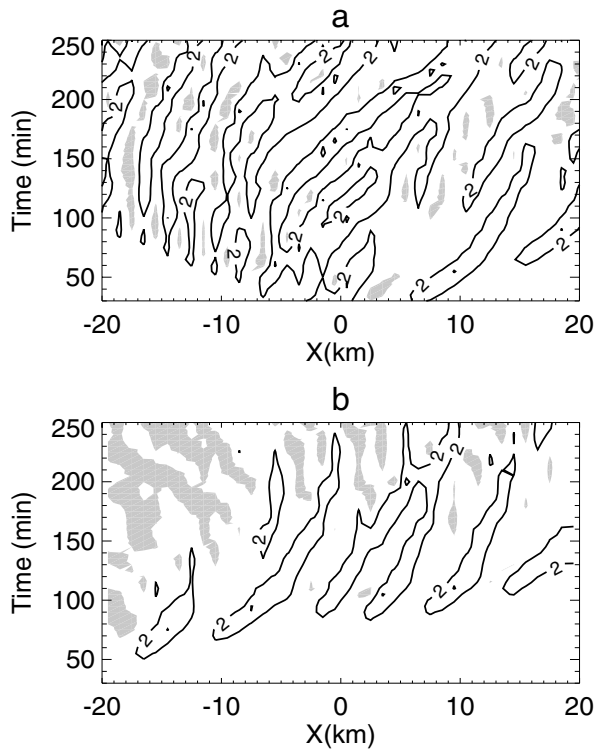

Fig. 6. The Hovmöller diagrams of $\overline{u}_z$ obtained from (a) the large domain simulation with periodic boundary conditions and (b) from the simulation with the LBC configuration CR. The negative contours are shaded.

However, as will be shown in section 3.3, this unrealistic flow reversal can be significantly reduced by enlarging the model domain.

We stated in section 2 that the radiation condition is applied on the normal velocities and the temperature in our model, and the three variables use the same phase speed C which is derived from the horizontal velocity field u. In theory, the phase speed C can also be determined independently from the temperature field. On the other hand, in Clark's (1979) work, only normal velocities were treated with a radiation scheme, while Miller and Thorpe (1981) used a radiation condition to compute the boundary values of the normal velocities and the temperature.

Two extra test runs have been designed to clarify the choice of C and the choice of a radiation condition for the normal velocities and the temperature. In one test run, the radiation condition is only applied on the normal velocities with C being calculated from u, while in the other, both the normal velocities and the temperature are treated with the radiation condition but with the phase speed for the normal velocities being calculated from u and the phase speed for the temperature being derived from the potential temperature field. Figure 7 depicts the Hovmöller diagrams of $\overline{u}_z$ calculated from these two test runs. The corresponding results from the standard run, which is identical with those two test runs except that the normal velocities and the temperature use the same phase speed C, are shown in Fig. 7c. The large domain periodic solution is given in Fig. 7d as a reference. The choice of using the same phase speed C in the radiation scheme is readily justified by Figs. 7c and 7d. The horizontal velocity begins to lose organization after 150 minutes of simulation when phase speeds for normal velocities and the temperature are different in the radiation scheme (Fig. 7a). If only the normal velocities are treated with a radiation condition, the solution is distorted after 80 minutes of simulation (Fig. 7b).

3.3 *Case 3: hilly terrain, diurnal surface thermal forcing*

Under many circumstances, convective systems are simulated in the context of diurnal thermal forcing, and convective motions may last for a long time. We have noted from the preceding examples that the numerical solutions change dramatically after a certain simulation time. The question of whether an LBC configuration performs well in simulations of diurnally thermally forced convective systems needs to be examined.

Under relatively light wind conditions, the model solution tends to be significantly contaminated by the boundary-induced errors and the selection of an appropriate LBC configuration is more important. In the subsequent simulations, although a geostrophic wind of 2 m s^{-1} is used, the results could be generalized to high wind conditions. Since we have noted in the last section that the LBC configuration CR is stable regardless of background wind conditions, the LBCs will be based on the CR configuration in the following simulations. The adoption of CR also makes it possible to incorporate inward propagating signals at the inflow boundary.

In theory, the larger the model domain, the more accurate the results are in simulations with open LBCs, so the results from the simulation with the largest domain can serve as a reference to the solutions over smaller domains, at least within a certain period of model simulation time. Here, three domains of lengths 40, 60, and 80 km were considered. All runs in this section begin at 0600 UTC and last for 24 hours. The position of a 200-m high and 10-km wide hill is fixed with respect to the inflow boundary for domains of different length. In fact, apart from the domain length and the LBCs, all other model parameters are kept unchanged in the following simulations. The six runs performed in this section are listed in Table 2. The

Table 2. Model configuration for six numerical experiments.

Simulations	Inflow condition	Outflow condition	Domain length (km)
S0	Periodic	Periodic	40 (Flat domain)
S1	Constant value	Radiation	40
S2	Specification	Radiation	40
S3	Specification	Radiation	60
S4	Specification	Radiation	80
S5	Specification	Radiation + Damp	60

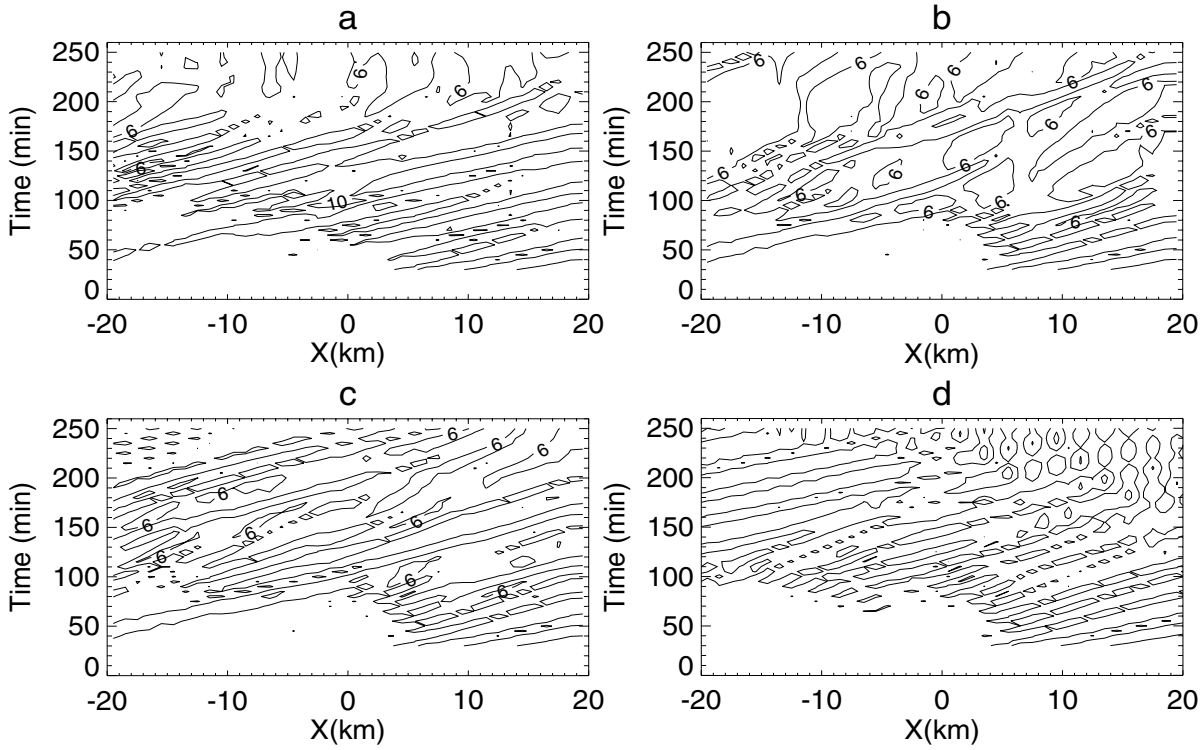

Fig. 7. The Hovmöller diagrams of column averaged horizontal velocity fields obtained from three simulations with the RR configuration: (a) only the normal velocities are treated with a radiation condition; (b) the normal velocities and the temperature use different phase speeds in the radiation scheme; (c) the normal velocities and the temperature use the same phase speed in the radiation scheme. The corresponding large domain periodic solution is also given for comparison (d).

specification inflow boundary condition means that the boundary values of the velocity fields are specified or reset every specified time period. The details of the Radiation + Damp outflow boundary condition will be discussed later.

Similar to the results in Fig. 6, the results from simulation S1 (not shown) indicate that the flow is reversed after some period of convection development. In fact, in the convective boundary with reasonably light background winds, a constant u at the inflow boundary is not physically justified. To amend this deficiency of the constant value condition, the velocity fields at the center of the model domain are gathered every minute from simulation S0. Then, in simulation S2, the velocity fields at the inflow boundary are reset every minute with the corresponding values from simulation S0. The approach, which is referred to as the specification boundary condition in Table 2, is actually equivalent to allowing the upstream modes from a uniform surface to propagate freely into the model domain. This configuration for the upstream boundary condition is justified both physically and numerically as for various simulations over hilly terrain, the physical problem is often related to observing how convective eddies from upstream are modified when they propagate over the underlying topography.

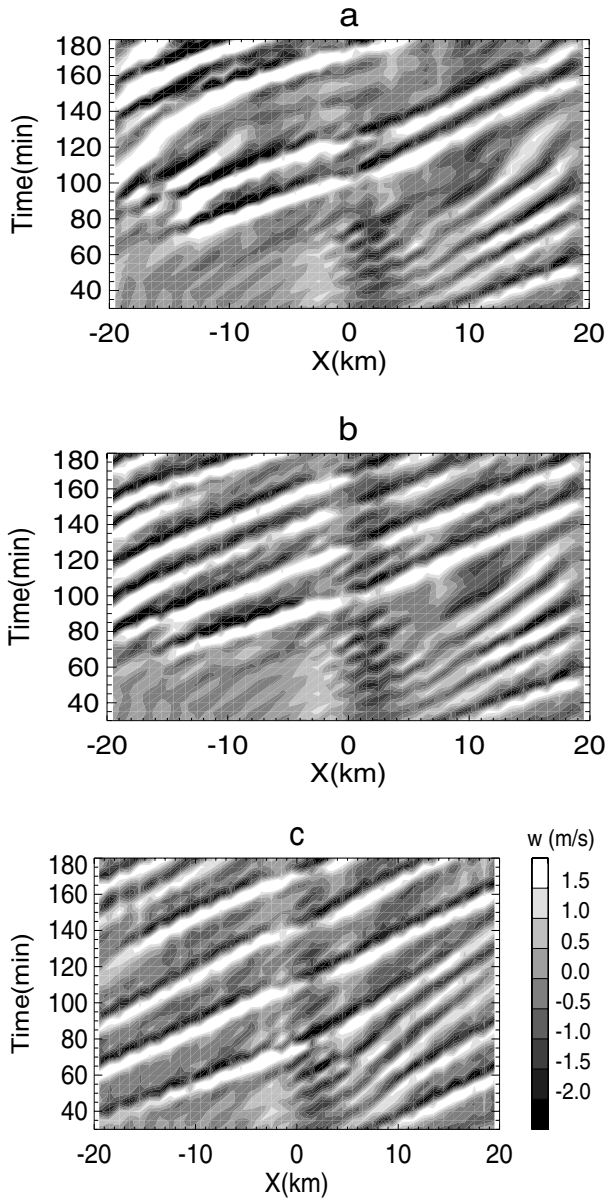

Fig. 8. The Hovmöller diagrams of vertical velocities from three hilly terrain simulations with (a) CR configuration, (b) SR, and (c) PP. The large scale geostrophic wind is 10 m s^{-1} and the model surface is constantly heated. The sections are all taken at the 600-m model level.

To verify the physical and numerical reliability of the specification boundary condition, three hilly terrain runs with constant thermal forcing are designed: one with a periodic LBC, the second with the CR configuration, and the last with the SR configuration, i.e., the specification inflow condition and the radiation outflow condition. Since under high wind conditions the radiation condition works relatively well, those test runs are performed with a large scale geostrophic wind of 10 m s^{-1} so that the effects of changing the inflow condition on the model results can be more clearly detected. The Hovmöller diagrams of vertical velocities from these three runs, which are only different in the LBC configuration, are displayed in Fig. 8. The convective features associated with the CR configuration (Fig. 8a) further confirm the result in the preceding section that the model may fail to produce steady convective features with open LBCs. As expected, the features in Fig. 8b are consistent with those over a periodic domain (Fig. 8c). It is apparent that the specification boundary condition at the inflow boundary gives a better vertical velocity field than the constant value condition does. A corresponding test run with a much broader horizontal domain length (i.e., 200 m) indicates that using a specification inflow condition not only allows time dependent variation of the upstream flow but also produces reasonable model results with a smaller horizontal model domain.

A few realizations of the vertical velocity field and the temperature field from simulation S2 are given in Fig. 9. One can see that strong updrafts near the inflow boundary remain there and the flow reversal is not diminished by the specification boundary condition. Also noticeable is a strong wave mode associated with the outflow boundary at 1700 UTC (Fig. 9b). This upward propagating wave mode seems to have enough energy to reach the upper boundary and be reflected again even though there is a Rayleigh damping layer for the upper boundary (Fig. 9c). The results here indicate that the flow reversal is caused indirectly by the two boundaries.

It is possible that the flow reversal may also be related to the mass flux correction applied at the outflow boundary when the constant value condition is used at the inflow boundary.

More information on the spurious flow reversal near the inflow boundary and the strong wave mode near the outflow boundary can be gained by enlarging the domain length of the simulation. Figure 11 gives the time and vertically averaged vertical velocity fields, $(\overline{w^2_{z,t}})^{1/2}$ for five simulations discussed in this study. The results from simulation S3 indicate that the flow reversal near the inflow boundary is significantly reduced and, as a result, the spurious strong updrafts are also greatly weakened. It should be noted that the spurious reflections at the outflow boundary like that in Fig. 9b still exist. The time when the convective features near the outflow boundary are significantly contaminated by the outflow boundary varies only slightly with different domain lengths. The points here can be further confirmed by the vertical velocity field from simulation S4 which is performed over an even broader domain of 80 km (Fig. 11).

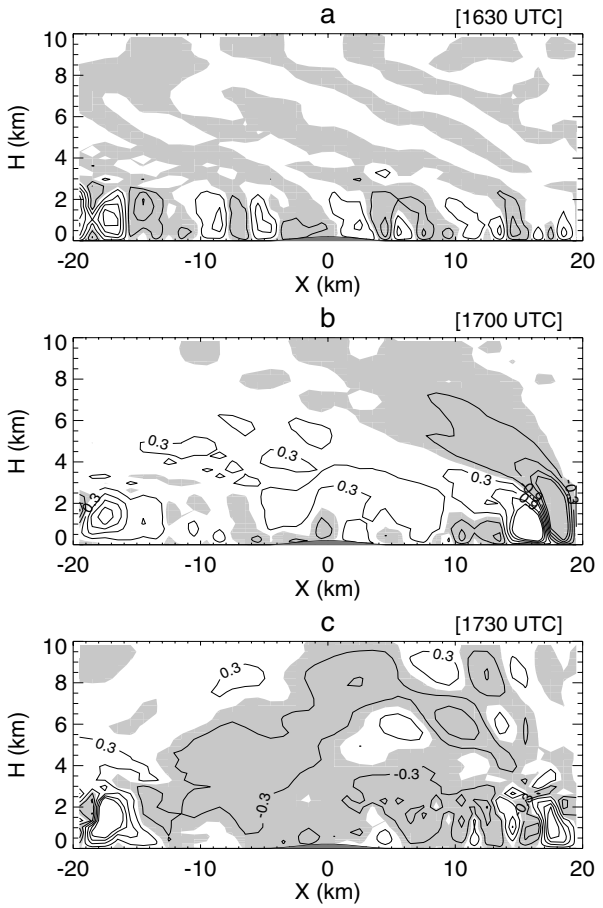

Fig. 9. Three sections of the instantaneous vertical velocity fields from simulation S2. The contour intervals are 0.6 m s^{-1}. The negative contours are shaded. The corresponding simulation times are marked on the top of each panel.

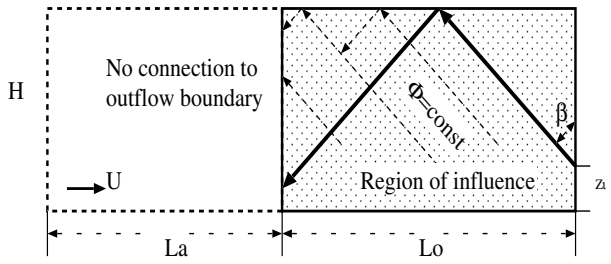

Fig. 10. The schematic diagram of the reflections caused by the boundaries and their influence region. The heavy solid arrows represent the reflection paths and light dotted arrows are constant phase lines. U stands for background wind and Φ is the phase angle.

The above analysis suggests that there are three factors which may be related to the reversed flow in simulations S1 and S2: convection itself and the reflection of the outflow boundary together will generate vertically and horizontally propagating gravity waves near the outflow boundary; the mass flux correction introduces more errors which tend to intensify the above processes so that upward propagating waves are able to reach the upper boundary and are further reflected; if the model domain is small enough for the secondary reflected waves to reach the inflow boundary, large errors may build up since the inflow boundary is not permeable. Figure 10 depicts the reflection paths associated with a boundary-related internal gravity wave. One can expect that the outflow boundary tends to affect model solutions within a distance of $L_{\rm o}$ from it. The solution within the area $L_{\rm a} \times H$ in Fig. 10 is less likely be influenced by the outflow boundary.

$L_{\rm o}$ is related to the domain depth, H, and the angle between gravity wave phase lines and the vertical, β through an approximate relation of $L_{\rm o} \approx 2(H-z_i)\tan\beta$, where z_i is the CBL (convective boundary layer) depth. Based on linear gravity wave theory, the angle of the phase lines to the local vertical can be estimated by $\cos\beta = 2\pi U/NL_x$, where L_x is the horizontal wavelength, and U and N are the background wind speed and Brunt-Väisälä frequency, respectively. As a result, the approximate domain length can be estimated by

$$L_{\rm o} = \frac{H - z_i}{\pi U}\sqrt{N^2L_x^2 - 4\pi^2U^2}\ .$$

If the model domain length L is large enough, i.e., $L \gg L_{\rm o}$, the reflections from the outflow boundary cannot reach the inflow boundary. Under such circumstances, the two lateral boundaries are disconnected, and the spurious convective eddies near the inflow boundary will disappear. In Fig. 9a, $H = 10$ km, $z_i \cong 2$ km, $\beta \cong 73°$; correspondingly, a rough estimate of $L_{\rm o}$ is 55 km. It is apparent that a 40-km domain is not large enough for simulation S2.

Although the effects of the lateral boundaries on the convective features far away from them become negligible when the model domain is large enough, the domain size is computationally limited for practical use. Another approach to minimize the effects of the outflow boundary on model results is to apply an absorbing condition. An approach, which is referred to as Radiation + Damp in Table 2, is proposed here: the model horizontal velocity u at the outflow boundary is first calculated using the Orlanski radiation scheme, then, a tendency modification scheme of Davies (1983) is performed on the horizontal velocity field within an eight point edge of the domain. The scheme actually employs Rayleigh damping within an eight grid point strip adjacent to the outflow boundary. Within the damping layer, the velocity u is calculated as

$$u_{j,n+1} = \tilde{u}_{j,n+1} - \gamma_j(\tilde{u}_{j,n+1} - u_b)\ . \qquad (17)$$

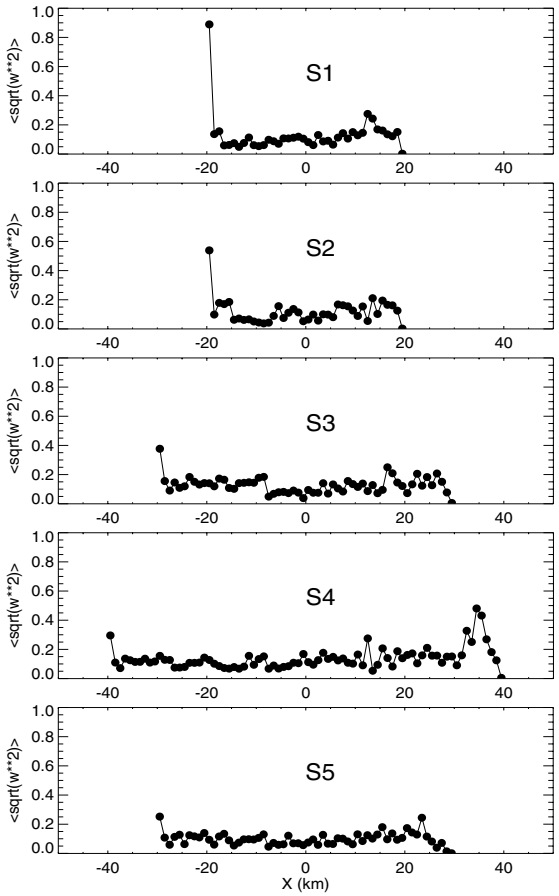

Fig. 11. The time and vertically averaged vertical velocity fields from simulation S1–S5.

Here, $\tilde{u}_{j,n+1}$ is an intermediate result which is first computed using the full equations, $u_{j,n+1}$ is the final result, and $u_{\rm b}$ is the initial boundary value, j is the coordinate index in the direction normal to the boundary and γ_j uses the values 0.02, 0.1, 0.25, 0.5, 0.75, 0.9, 0.98, and 1.0 as j approaches the outside edge of the damping layer.

It is evident from Fig. 11 that the errors at the inflow boundary are gradually reduced from simulation S0 to S5. The spurious convective eddies near both boundaries are largely diminished with the mixed outflow boundary condition, even with a model domain of 60 km. The boundary errors at the outflow boundary are less significant than those at the inflow boundary in Fig. 11, but it bears repeating that the small errors at the outflow boundary may give rise to large errors at the inflow boundary when the horizontal model domain is not large enough.

It is appropriate at this point to check the effects of the LBCs on the simulated convective boundary layer depth. Figure 12 displays the instantaneous potential temperature profiles 10-km downstream of the hill which were gathered at the simulation times 1500, 1600, and 1700 UTC. Note that there are no significant differences in the CBL depth between the different simulations until 1500 UTC. However, the differences become quite evident at 1600 and 1700 UTC. The effects of the domain length on the CBL depth are visible, but are less significant than the effects of the LBCs. At 1700 UTC, there is an over 1-km difference in the CBL depth between simulation S1 and S5, while there is no significant difference between S1 and S4. The differences in the profiles are mainly caused by the anomalous eddy structures near the outflow boundary seen in Fig. 9. With regard to deep convective initiation, a 1-km difference in the CBL depth may make a big difference in subsequent convection development under certain atmospheric conditions.

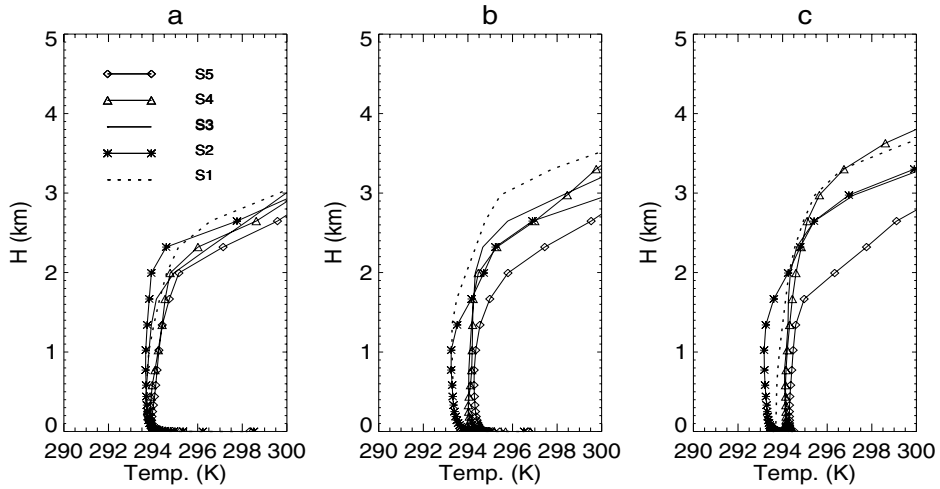

Fig. 12. The instantaneous potential temperature profiles 10 km downstream of the hill gathered from simulations S1–S5. (a) 1500 UTC; (b) 1600 UTC; (c) 1700 UTC.

4. Conclusion and remarks

It is known that there are various problems associated with open boundary conditions in the mesoscale simulation of convection over topography, and easily applicable theoretical results in this particular field have not been obtained yet. In many convective cloud simulations, the best results may not be produced by improving the accuracy or the permeability of the boundary conditions but rather by tuning the boundary conditions to produce a reflection or a computational error most closely simulating the inward propagating modes that may develop and interact with convective motions within the model domain. Attempts to find an optimal LBC configuration for a given physical problem are of some practical use since a perfect boundary condition can never be achieved.

Although there is no single LBC configuration that is suitable for every physical problem, our model results indicate that the configuration CR is appropriate in most cases. In simulations with constant thermal forcing at the model surface, the numerical solution is only reliable within a certain period of simulation time. This critical time t_c may depend on LBCs, domain size, and spatial resolution as well as the physical problem under consideration. The simulations in this study suggest that within about 150 minutes, the model results are at least numerically reliable regardless of the LBCs and background winds.

The superiority of using a radiation boundary condition at both boundaries is not well pronounced under light wind conditions since no distinct waves are generated in such circumstances and the uncertainties in the specification of phase speed C become significant. However, at the outflow boundary, a radiative condition is quite necessary under both high and light background winds. On the other hand, the model results with both the normal velocities and the temperature being treated with a radiation condition are relatively better than those with only the normal velocities using a radiation condition. The model solution is more stable when both the normal velocities and the temperature use the same phase speed in the radiation scheme rather than using different ones.

In time dependent convection simulations, such as simulations with diurnal thermal forcing at the model surface, the combined use of a radiation scheme and a damping scheme is necessary at the outflow boundary to diminish boundary-induced errors. The specification inflow boundary condition proposed in this study makes it possible to use a smaller domain in the upstream of a hill. For simulations with open LBCs, the minimum horizontal domain length needs to be selected carefully according to domain depth H and β, the angle between gravity wave phase lines and the vertical. If the model domain is not large enough to disconnect reflections between boundaries, significant errors can be generated. Note that we have not discussed cases where the basic flow has vertical directional shear. These issues need to be further investigated.

Acknowledgments. Drs. Doug Parker, Andrew Ross, and Simon Vosper provided many useful comments on the results and the manuscript. The first author was supported by an Overseas Research Scholarship. The authors would like to thank the two anonymous reviewers for improving the clarity of the paper. This work was supported by the National Natural Science Foundation of China under Grant No. 40233031.

REFERENCES

Clark, T. L., 1977: A small-scale dynamic model using a terrain-following transformation. *J. Comput. Phys.*, **24**, 186–215.

Clark, T. L., 1979: Numerical simulations with a three-dimensional cloud model: Lateral boundary condition experiments and multicellular severe storm simulations. *J. Atmos. Sci.*, **36**, 2191–2215.

Davies, H. C., 1983: Limitations of some common lateral boundary schemes used in regional NWP models. *Mon. Wea. Rev.*, **111**, 1002–1012.

Deardorff, J. W., 1974: Three-dimensional numerical study of the height and mean structure of the heated planetary boundary layer. *Bound. Layer Meteor.*, **7**, 81–105.

Deardorff, J. W., 1978: Efficient prediction of ground-surface temperature and moisture, with inclusion of a layer of vegetation. *J. Geophys. Res.*, **83**, 1889–1903.

Durran, D. R., and J. B. Klemp, 1983: A compressible model for the simulation of moist mountain waves. *Mon. Wea. Rev.*, **111**, 2341–2361.

Durran, D. R., M. Yang, D. N. Slinn, and R. G. Brown, 1993: Toward more accurate wave-permeable boundary conditions. *Mon. Wea. Rev.*, **121**, 604–620.

Klemp, J. B., and R. B. Wilhelmson, 1978: The simulation of three-dimensional convective storm dynamics. *J. Atmos. Sci.,* **35**, 1070–1096.

Mason, P. J., 1987: Diurnal variations in flow over a succession of ridges and valleys. *Quart. J. Roy. Meteor. Soc.*, **113**, 1117–1140.

Miller, M. J., and A. J. Thorpe, 1981: Radiation conditions for the lateral boundaries of limited-area numerical models. *Quart. J. Roy. Meteor. Soc.*, **107**, 615–628.

Miranda, P. M. A., and I. N. James, 1992: Nonlinear three-dimensional effects on gravity-wave drag: Splitting flow and breaking waves. *Quart. J. Roy. Meteor. Soc.*, **118**, 1057–1081.

Orlanski, I., 1976: A simple boundary condition for unbounded hyperbolic flows. *J. Comput. Phys.*, **21**, 251–269.

Pearson, R. A., 1974: Consistent boundary conditions for numerical models of systems that admit dispersive waves. *J. Atmos. Sci.*, **31**, 1481–1489.

Raymond, W. H., and H. L. Kuo, 1984: A radiation boundary condition for multi-dimensional flows. *Quart. J. Roy. Meteor. Soc.*, **110**, 535–551.

Stephens, G. L., 1984: The parameterization of radiation for numerical weather prediction and climate models. *Mon. Wea. Rev.*, **112**, 826–867.

Sommerfeld, A., 1949: *Partial Differential Equations in Physics*. Academic Press, 335pp.

Sundstrom, A., and T. Elvius, 1979: Computational problems related to limited area modeling. *Numerical Methods Used in Atmosphere Models*, GARP Publication Series, Vol. 11, chap. 7, No. 17.

Wood, N., 1995: The onset of separation in neutral, turbulent flow over hills. *Bound.-Layer Meteor.*, **76**, 137–164.

Wood, N., and P. Mason, 1991: The influence of static stability on the effective roughness length for momentum and heat transfer. *Quart. J. Roy. Meteor. Soc.*, **117**, 1025–1056.